

THE DETECTION OF THE SOURCE OF ACOUSTICAL NOISE IN TWO DIMENSIONS*

THOMAS DELILLO[†], VICTOR ISAKOV[†], NICOLAS VALDIVIA[†], AND LIANJU WANG[†]

Abstract. We consider the problem of detecting the source of acoustical noise inside the cabin of a midsize aircraft from measurements of the acoustical pressure field inside the cabin. Mathematically this field satisfies the Helmholtz equation. In this paper we consider the model two-dimensional case. We show that any regular solution of this equation admits a unique representation by a single layer potential, so that the problem is reduced to the solution of a linear integral equation of the first kind. We prove uniqueness of reconstruction and obtain a sharp stability estimate. Finally, for two geometries and sources of noise simulating the cabin of the aircraft and two engines, we give results of the numerical solution of this integral equation, comparing regularization by the truncated singular value decomposition and the conjugate gradient method.

Key words. inverse problems, acoustics

AMS subject classifications. 35R30, 76Q05

PII. S0036139900367152

1. Introduction. We consider the problem of identifying the source of the acoustical noise and the normal velocity of the sound on the surface of a domain Ω . The acoustical field u of frequency k in Ω satisfies the Helmholtz equation

$$(1) \quad \Delta u + k^2 u = 0 \quad \text{in } \Omega.$$

In our application Ω is the cabin of an aircraft. Acoustical sensors are located on a surface Γ_0 inside the cabin. The sensors measure the field u and the problem is to recover u inside Ω from these measurements and, in particular,

$$(2) \quad v = \partial_\nu u \quad \text{on } \Gamma,$$

which is the boundary of Ω . Here ν is the unit exterior normal to Γ . We will represent u by the single layer potential

$$(3) \quad u(x) = \int_\Gamma K(x, y) \phi(y) d\Gamma(y), \quad x \in \Omega,$$

where $K(x, y)$ is the free space radiating fundamental solution to the Helmholtz equation. Now our problem is reduced to solving the linear integral equation

$$(4) \quad \int_\Gamma K(x, y) \phi(y) d\Gamma(y) = \Phi(x), \quad x \in \Gamma_0.$$

After solving this equation for ϕ one can find the normal velocity from the formula

$$(5) \quad v(x) = \phi(x)/2 + \int_\Gamma \nabla_x K(x, y) \cdot \nu(x) \phi(y) d\Gamma(y), \quad x \in \Gamma,$$

*Received by the editors January 19, 2000; accepted for publication (in revised form) October 6, 2000; published electronically May 10, 2001. This research was supported by NSF grant DMS 9803816 and the Cessna Aircraft Company.

<http://www.siam.org/journals/siap/61-6/36715.html>

[†]Department of Mathematics and Statistics, Wichita State University, Wichita, KS 67260-0033 (delillo@twsuvm.uc.twsu.edu, isakov@twsuvm.uc.twsu.edu, valdivia@math.twsu.edu, lwang@twsuvm.uc.twsu.edu).

which follows from (3) and the jump relations for the normal derivative of single layer potentials. This approach in principle allows us to handle general domains Ω . Methods such as those developed in [4], [18], [19], [21], and [20] are applicable only to very special (rotationally symmetric) Ω when the Green's function of the Neumann problem for the Helmholtz equation can be found explicitly. More recently these methods were adjusted to more general geometries related to the cabin of an aircraft [21]. In these cases one still needs knowledge of the Neumann Green's function which is quite difficult to compute. Another widely used approach [3], [13], [22] is based on a system of two integral equations for the unknown pressure and the normal velocity (the Helmholtz–Kirchhoff equations) and instead of using the complicated Neumann Green's function it utilizes the simple free-space fundamental solution. We propose to solve only one integral equation (4) and we expect our method to be more economical. We think that the representation (4) is physical and reflects the essence of the problem where one is looking for the source of noise: the function ϕ can be interpreted as the density of a source distribution. The existing methods are used mostly for solving practical problems and, as a rule, they are not justified mathematically. We give a rigorous justification of our method including quite sharp and explicit stability estimates for reconstruction of pressure and normal velocity.

The realistic problem is three-dimensional and not well posed (see [6]). This fact, combined with the need to find about 1000 unknowns in the discretized problem, creates serious computational difficulties. To test our algorithms and to compare different approaches we first will consider a two-dimensional version of this problem. In a forthcoming paper, we will handle the complete three-dimensional case. Most of the theoretical results of this paper are also valid in the three-dimensional case with rotational symmetry.

In section 2 of this paper we show that any (regular) solution to the Helmholtz equation (disregarding possible eigenvalues of the Dirichlet or Neumann problems in Ω) can be uniquely represented by a single layer potential. We use this representation to record these solutions. To find the normal velocity (2) it suffices to compute an integral with a bounded kernel. Section 3 contains stability estimates for recovery of u on Ω or ϕ on Γ . These conditional estimates are of logarithmic type and we attempt to find explicit formulas for constants in the estimates for the particular case when Ω is the disk $|x| < r_1$ and Γ_0 is the circle $|x| = r_0$. Section 4 exposes the results of our numerical experiments.

2. Single layer potential representation. We will characterize the source of an acoustical field $u(x)$ in $\Omega \subset \mathbb{R}^2$ by its surface density ϕ on Γ . In other words, for a solution u to (1) we would like to find a function ϕ such that (3) holds. Here

$$(6) \quad K(x, y) = i/4 H_0^{(1)}(k|x - y|)$$

is the well-known fundamental solution to the Helmholtz equation in the plane satisfying the Sommerfeld radiation condition

$$\lim_{r \rightarrow \infty} r^{1/2}(\partial_r u - iku)(x) = 0,$$

where $r = |x|$. $H_0^{(1)}(s)$ is the Hankel function of the first kind (see [6]).

We will assume that $\partial\Omega \in C^{1,1}$, which means that tangent to $\partial\Omega$ at x is a Lipschitz function of x . By $H_{(k)}(\Omega)$ we will denote the Sobolev space of functions u in Ω with the partial derivatives $\partial^\alpha u$ of order $|\alpha| \leq k$ in $L^2(\Omega)$. The norm in this

space is denoted by $\|u\|_{(k)}(\Omega)$ and the norm in $L^2(\Omega)$ is

$$\|u\|_2(\Omega) = \left(\int_{\Omega} |u(x)|^2 dx \right)^{\frac{1}{2}}.$$

The existence of the representation (3) is guaranteed by the following.

THEOREM 2.1. *For any solution $u \in H_{(2)}(\Omega)$ to the Helmholtz equation (1) there is an unique function ϕ such that (3) holds. Moreover, for some constant C depending only on Ω we have*

$$(7) \quad \|\phi\|_2(\Gamma) \leq C\|u\|_{(2)}(\Omega)$$

and if in addition $u \in C^{1+\lambda}(\bar{\Omega}), 0 < \lambda < 1$, then

$$(8) \quad C^{-1}|u|_{1+\lambda}(\Omega) \leq |\phi|_{\lambda}(\Gamma) \leq |u|_{1+\lambda}(\Omega).$$

Proof. We will first show uniqueness of ϕ such that (3) holds. By using the jump relations for the normal derivative of single layer potentials [6], [15] we obtain

$$(9) \quad \partial_{\nu}u^{-} + iu^{-} = \phi/2 + W\phi + iS\phi \quad \text{on } \Gamma.$$

By trace theorems the left side is well defined and contained in $L^2(\Gamma)$. We will consider (9) as an integral equation with respect to ϕ . To establish the uniqueness of ϕ it suffices to show that the function ϕ is zero when the left side in (9) is zero. Letting $S = S\phi$ we will then have

$$(10) \quad \phi = -2W\phi - i2S\phi \quad \text{on } \Gamma.$$

By the smoothing properties of single and double layer potentials ([11, p. 19] or [15]) the right side in (10) is in $C^{\gamma}(\Gamma)$ for any $\gamma < 1$. Hence the density function ϕ itself is Hölder continuous. Again by regularity properties of single layer potentials $S\phi \in C^1(\bar{\Omega})$.

To show that $\phi = 0$ it suffices to use the following.

LEMMA 2.2. *If $(\Delta + k^2)u = 0$ in a bounded Lipschitz domain Ω , $u \in H_{(1)}(\Omega)$, and $\partial_{\nu}u + iu = 0$ on $\partial\Omega$, then $u = 0$ in Ω .*

Proof. The definition of the (generalized) $H_{(1)}$ -solution to the Helmholtz equation in Ω gives

$$\int_{\Omega} (\nabla u \cdot \nabla \bar{u} - k^2 u \bar{u}) = - \int_{\partial\Omega} \partial_{\nu} u \bar{u}.$$

The boundary condition implies that $\partial_{\nu}u = -iu$. Hence in the last integral equality the right side is purely imaginary and the left side is real. Hence they are both zero, and $u = 0$ on $\partial\Omega$. Using the boundary condition again we conclude that $\partial_{\nu}u = 0$ on $\partial\Omega$.

Since $u = 0$ on the Lipschitz surface $\partial\Omega$ its zero extension u^* onto $\mathbb{R}^2 \setminus \Omega$ is an $H_{(1)}(\mathbb{R}^2)$ -function. Using the definition of a generalized solution and the integration by parts formula (valid for Lipschitz domains and $H_{(1)}$ -functions on such domains) we conclude that u^* solves the Helmholtz equation on the whole plane. Since $u^* = 0$ outside Ω by the uniqueness of the continuation it is zero in Ω . So $u = 0$ in Ω .

The proof is complete. \square

This lemma is well known for $u \in C^1(\bar{\Omega})$ [5, Theorem 3.33], and we give a proof for completeness.

Now we return to the proof of Theorem 2.1.

As shown before in Lemma 2.2 the single layer potential $S = S\phi$ satisfies the regularity conditions of this lemma, solves the Helmholtz equation in Ω and, according to 10 and the jump relations $\partial_\nu S + iS = 0$, on Γ . By Lemma 2.2 we have $S = 0$ on Ω . As known [11], [15], $S = S\phi$ is continuous on the plane and according to [6] it satisfies the Sommerfeld radiation condition at infinity. Since $S = 0$ on $\partial\Omega$ by the uniqueness in the exterior Dirichlet problem we conclude that $S = 0$ outside Ω (see [6]). Using again the jump relations for the normal derivatives of single layer potentials we conclude that $\phi = 0$ on Γ . In particular, we have uniqueness of a solution to the integral equation (9) with respect to $\phi \in L^2(\Gamma)$. Due to the known (see [15]) smoothing properties of the single and double layer potentials the operators $W\phi$ and $S\phi$ are compact from $L^2(\Gamma)$ into itself. Hence the integral equation (9) is Fredholm and the uniqueness of its solution implies its existence, so for any $u \in H_{(2)}(\Gamma)$ there is a unique solution $\phi \in L^2(\Gamma)$ to (9).

Now we claim that (3) holds. Indeed, let S be the single layer potential $S\phi$. From jump relations for normal derivative of single layer potentials and from (9) we conclude that $\partial_\nu(u^- - S) + i(u^- - S) = 0$ on Γ . Also the function $u^- - S$ satisfies the Helmholtz equation (1) in Ω and is in $H_{(1)}$ because of regularity properties of single layer potential of a L^2 -density. By Lemma 2.2 we have $u^- = S$ on Ω .

Now we will derive the bound (7). Since the integral equation (9) has a solution for any left side in $L^2(\Gamma)$ and the operators in the right side are continuous in $L^2(\Gamma)$ by the Banach closed graph theorem the solution operator is continuous from $L^2(\Gamma)$ into $L^2(\Gamma)$. By trace theorems the operator mapping u in Ω into its trace on Γ is bounded from $H_{(2)}(\Omega)$ into $L^2(\Gamma)$, so we have the bound (7).

The bounds (8) can be proven similarly, when we replace Sobolev space by Hölder space and use known regularity properties of potentials and solutions to elliptic boundary value problems in these spaces collected for example in [11, section 1.6].

Observe that Theorem 2.1 is well known if k is not a Dirichlet or Neumann eigenvalue of the Laplacian in Ω [5, Theorems 3.16 and 3.30]. We do not assume that k is not such an eigenvalue.

3. Uniqueness and stability for the inverse source problem. In this section we will derive sharp stability estimates for our inverse problem. The uniqueness and stability problem is decomposed into the (well-posed) Dirichlet problem for the Helmholtz equation in the domain Ω_0 bounded by Γ_0 and the problem of the continuation of a solution to this equation from Ω_0 onto Ω . The Dirichlet problem, however, can have eigenvalues (in particular for our specific application) which are relatively easy to find for circular Ω and to bound from above and below for more general domains by using monotonicity of Dirichlet eigenvalues with respect to a domain. Nonuniqueness generated by these eigenvalues cannot be avoided, and away from them the Dirichlet problem is stable in classical Sobolev (or Hölder) spaces (with loss of one derivative). The problem of continuation of solutions of elliptic equations is notoriously unstable. However, assuming that $\|u\|_2(\Omega) < M_0$, one has the conditional Hölder-type estimate

$$(11) \quad \|u\|_{(k)}(\Omega_1) < CM_0^{1-\theta} \|u\|_2^\theta(\Omega_0),$$

where C, θ depend on $\Omega, \Omega_0, k, 0 < \theta < 1$, and the distance from Ω_1 to Γ . We refer for proofs to [12, sections 3.2, 3.3]. More delicate stability estimates of $\|u\|_2(\Omega)$ need some

further constraints, like the bound $\|u\|_{(1)}(\Omega) < M_1$. One can then obtain logarithmic conditional stability estimates

$$(12) \quad \|u\|_2(\Omega) \leq C/|\log(\|u\|_2(\Omega_0))|^\theta,$$

where C, θ depend on Ω, Ω_0, M_1, k . In applied situations the bounds M_0, M_1 can be available from the physical nature of the problem (like boundedness of the potential energy M_1). The stability estimates (11), (12) imply convergence rates for certain regularization algorithms for the numerical solution. However, in the general situation explicit bounds for C, θ are not known. In this section we will obtain rather sharp bounds for these constants when Ω is the disk $\Omega(r_1)$ defined as $|x| < r_1, r_1 \leq 1$, and Ω_0 is its subdisk $\Omega(r_0)$.

THEOREM 3.1. *Let u be a solution to the Helmholtz equation (1) in the disk $\Omega(r_1)$ and*

$$(13) \quad \|u\|_2(\Omega(r_1)) \leq M_0, \|\nabla u\|_2(\Omega(r_1)) \leq M_1.$$

Then

$$(14) \quad \frac{r_0}{r} \|u\|_2^2(\partial\Omega(r)) \leq C_1(r)\varepsilon^2 + C_2\varepsilon^{2\theta}, \quad r < r_1,$$

where $\theta = (\ln r_1 - \ln r)/(\ln r_1 - \ln r_0)$, and

$$(15) \quad \|u\|_2^2(\partial\Omega(r_1)) \leq C_1(r_1)\varepsilon^2 + C_4\varepsilon_1 - C_3\varepsilon_1 \ln(\varepsilon_1),$$

where $\varepsilon = \|u\|_2(\partial\Omega(r_0))$, $C_1(r) = \max|J_n(kr)/J_n(kr_0)|^2$ over $|n| \leq n_1, n_1 = [k^2 r_1^2/2 - 1]$, $C_2 = 4((1 + \frac{2}{r_1})M_0^2 + M_1^2)$, and in the logarithmic bound $\varepsilon_1 = -\frac{1}{\ln \varepsilon}$, $C_3 = \max(k^2 M_0^2, M_1^2) \ln \frac{r_1}{r_0}$, and $C_4 = C_3(1 - \ln \frac{C_3 r_0}{2C_2})$.

In the proof we will use the following known expansion of a solution u to (1):

$$(16) \quad u(r, \varphi) = \sum_{-\infty}^{\infty} J_n(kr)u_n e^{in\varphi}, \quad \varphi \in I = (0, 2\pi),$$

where

$$J_n(t) = \sum_{p=0}^{p=+\infty} (-1)^p / (p!(n+p)!) (t/2)^{n+2p}, \quad n = 0, 1, 2, \dots, J_{-n} = J_n,$$

is the n th Bessel function and (r, φ) are the polar coordinates in the plane. This expansion shows that nonuniqueness can occur only when the function $J_n(kr_0) = 0$ for some $n = 1, 2, \dots$.

In addition we will make use of the following simple lemma.

LEMMA 3.2. *Under the condition (13) we have*

$$(17) \quad \int_{|x|=r} |u|^2 \leq \left(\left(1 + \frac{2}{r}\right) M_0^2 + M_1^2 \right), \quad \operatorname{Re} \int_{|x|=r} \partial_\nu u \bar{u} \leq \max(k^2 M_0^2, M_1^2)$$

provided $\Delta u + k^2 u = 0$ in Ω .

Proof. From the integration by parts formula we have

$$r \int_{|x|=r} u \bar{u} = \int_{|x|<r} (r \partial_r |u|^2 + 2|u|^2) \leq \int_{|x|<r} (2r|u||\nabla u| + 2|u|^2) \leq \int_{|x|<r} (r|\nabla u|^2 + (r+2)|u|^2)$$

and by using (13) we have the first bound of the lemma.

Again using integration by parts, we have

$$0 = \int_{|x|<r} (\Delta u + k^2 u)\bar{u} = \int_{|x|=r} (\partial_\nu u)\bar{u} - \int_{|x|<r} (\nabla u \cdot \nabla \bar{u} - k^2 u\bar{u})$$

and we similarly arrive at the second bound of this lemma.

The proof is complete. \square

Proof of Theorem 3.1. We let $t = kr$. Due to the choice of n_1 we have

$$(18) \quad J_n(t) = (t/2)^n / (n!)(1 - \rho_n(t)),$$

where $|\rho_n(t)| < \frac{1}{2}$ when $n_1 \leq |n|$. Indeed,

$$\begin{aligned} \rho_n(t) &= \frac{t^2}{4} \sum_{p=0}^{\infty} \frac{1}{1 \dots (2p+1)(n+1) \dots (n+2p+1)} \left(1 - \frac{1}{(2p+2)(n+2p+2)} t^2/4\right) (t^2/4)^{2p} \\ &\leq \frac{t^2}{4(n+1)} \left(\sum_{p=0}^{\infty} \frac{1}{(p)!} \left(\frac{t^2}{8(n+2)}\right)^{2p} - \frac{t^2}{8(n+2)} \right) \leq \frac{t^2}{4(n+1)} \left(e^{(\frac{t^2}{8(n+2)})^2} - \frac{t^2}{8(n+2)} \right). \end{aligned}$$

When $1/3 < \frac{t^2}{4(n+1)} < 1/2$ the last expression is less than $1/2(e^{1/16} - 1/6) < 1/2$.

When $\frac{t^2}{4(n+1)} < 1/3$ it is less than $1/3e^{1/36} < 1/2$ as well. The inequality $\frac{t^2}{4(n+1)} < 1/2$ holds when $n_1 \leq |n|$.

Since the complex exponents are orthogonal in $L^2(0, 2\pi)$ we have from (16) that

$$(19) \quad \|u(t/k, \cdot)\|_2^2(0, 2\pi) = f_0(t) + f_1(t),$$

where

$$f_0(t) = 2\pi \sum_{|n| \leq n_1} |u_n|^2 J_n^2(t)$$

and f_1 is the similar sum over $n_1 < |n|$.

From the definition of f_0 and from the choice of C_1 we have

$$(20) \quad f_0(t) \leq C_1(r) f_0(t_0).$$

To obtain a bound for f_1 we will estimate it by the simpler function

$$F(t) = 2\pi \sum_{n_1 < |n|} |u_n|^2 2^{-2n} (n!)^{-2} t^{2n}.$$

From (18) and (19) it follows that

$$(21) \quad 1/4F(t) \leq f_1(t) \leq F(t).$$

It is not hard to check that the function $h(s) = F(e^s)$, $s = \ln t$ is logarithmically convex: $h'^2 \leq h^{(2)}h$ [12, p. 41]. Hence

$$h(s) \leq (h(s_0))^{(s_1-s)/(s_1-s_0)} (h(s_1))^{(s-s_0)/(s_1-s_0)}$$

and using (21) twice yields

$$f_1(t) \leq F(t) \leq (F(t_0))^\theta (F(t_1))^{1-\theta} \leq 4(f_1(t_0))^\theta (f_1(t_1))^{1-\theta}$$

with $\theta = (s_1 - s)/(s_1 - s_0)$. Observing that due to Lemma 3.2

$$f_1(t) \leq r^{-1} \int_{|x|=r} |u|^2 \leq \frac{1}{r} \left(\left(1 + \frac{2}{r}\right) M_0^2 + M_1^2 \right)$$

and using (20) we obtain the first (Hölder) conditional stability estimate (14).

To obtain the logarithmic bound we will in addition make use of the second bound of Lemma 3.2. From (13) and (19) one can see that

$$|f_1'| \leq \frac{2}{kr} |\operatorname{Re} \int_{|x|=r} \partial_\nu u \bar{u}| \leq \frac{2}{kr} \max(k^2 M_0^2, M_1^2).$$

By the mean value theorem

$$f_1(e^{s_1}) = f_1(e^s) + f_1'(e^{s_2}) e^{s_2} (s_1 - s) \leq \frac{C_2}{r_0} \varepsilon^{2\theta} + 2C_3\theta, \quad s < s_2 < s_1,$$

where we have used the above bound for $f_1(t)$ and let $C_3 = \max(k^2 M_0^2, M_1^2) \ln(r_1/r_0)$. The minimum of the right side with respect to $\theta \in [0, 1]$ is achieved at

$$\theta = -\frac{\varepsilon_1}{2} \ln \frac{C_3 r_0}{2C_2} - \frac{\varepsilon_1}{2} \ln \varepsilon_1, \quad \varepsilon^{2\theta} = \frac{C_3 r_0}{2C_2} \varepsilon_1,$$

where $\varepsilon_1 = -\frac{1}{\ln \varepsilon}$, provided ε is small. After substitution into the minimized expression we obtain (15).

THEOREM 3.3. *Assume that in addition to (13) we have*

$$(22) \quad \|\nabla^2 u\|_2(\Omega(r_1)) \leq M_2.$$

Then

$$\frac{r_0}{r} \|\partial_r u\|_2^2(\partial\Omega(r)) \leq C_{10} \varepsilon_2^2 + C_{11} \varepsilon_2^{2\theta}$$

with $C_{10} = C_1(r)M$, $M = k^2 \max(\frac{|J'_n(kr_0)|^2}{n^2 |J_n(kr_0)|^2}, \frac{16}{r_0^2}) + r_0^{-2}$ over $|n| \leq n_1 + 1$, $C_{11} = 4((1 + \frac{2}{r_1})M_1^2 + M_2^2)M$, $\varepsilon_2 = (3(M_0^2 + 2r_0^2 M_1^2 + r_0^4 M_2^2))^{1/3} \varepsilon^{1/3}$, and

$$\|\partial_r u\|_2^2(\partial\Omega(r_1)) \leq C_{10} \varepsilon_2^2 + C_9 \varepsilon_3 - C_8 \varepsilon_3 \ln(\varepsilon_3)$$

with $\varepsilon_3 = -\frac{1}{\ln M^{\frac{1}{2}} \varepsilon_2}$, $C_8 = \max(k^2 M_1^2, M_2^2) \ln \frac{r_1}{r_0}$, and $C_9 = C_8(1 - \ln \frac{C_8}{2C_7})$.

To prove Theorem 3.3 we need the following result about the explicit bound of norm of the trace operator in Sobolev spaces.

LEMMA 3.4. *We have*

$$(23) \quad \|f\|_{(1/2)}^2(\partial\Omega(r)) \leq 3r^2 \|\nabla f\|_2^2(\Omega(r)) + 3\|f\|_2^2(\Omega(r))$$

and

$$(24) \quad \|f\|_{(3/2)}^2(\partial\Omega(r)) \leq 3\|f\|_2^2(\Omega(r)) + 6r^2 \|\nabla f\|_2^2(\Omega(r)) + 3r^4 \|\nabla^2 f\|_2^2(\Omega(r)).$$

Proof. We will use the formulas

$$f(r, \varphi) = \sum f_n^\bullet(r) e^{in\varphi}, \quad \|f\|_{(k)}^2(\partial\Omega(r)) = 2\pi r \sum |f_n^\bullet|^2 (n^2 + 1)^k = \int_{\partial\Omega(r)} A^{\frac{k}{2}} \overline{A^{\frac{k}{2}} f},$$

where

$$A^k f(\varphi) = \sum f_n^\bullet (n^2 + 1)^k e^{in\varphi}.$$

To prove (23) we observe that as in the proof of Lemma 3.2 the left side in (23) equals

$$\begin{aligned} \int_{\partial\Omega(\rho)} A^{1/4} f \overline{A^{1/4} f} &= \frac{1}{\rho} \int_{\Omega(\rho)} (r \partial_r (A^{1/4} f \overline{A^{1/4} f}) + 2A^{1/4} f \overline{A^{1/4} f}) \\ &= 2\pi \int_0^\rho \left(\sum r^2 (\partial_r |f_n^\bullet(r)|^2 (n^2 + 1)^{1/2} + 2r |f_n^\bullet|^2 (n^2 + 1)) \right) dr \\ &\leq 2\pi \int_0^\rho r \sum (r^2 |\partial_r f_n^\bullet(r)|^2 + 3 |f_n^\bullet(r)|^2 (n^2 + 1)) dr. \end{aligned}$$

Here we have written the integral over $\Omega(r)$ in the polar coordinates (r, φ) , used the definition of A^k , the Parseval equality for the Fourier series, and the identity $\partial_r |f|^2 = 2\text{Re}((\partial_r f) \overline{f})$. Using the Parseval equality again we write the last integral as

$$\int_0^\rho r \left(\int_0^{2\pi} (r^2 |\partial_r f|^2 + 3 |\partial_\varphi f|^2 + 3 |f|^2) \right) \leq 3\rho^2 \|\nabla f\|_2^2(\Omega(\rho)) + 3\|f\|_2^2(\Omega(\rho)),$$

where we have used the equality $\nabla = (\partial_r, r^{-1} \partial_\varphi)$. This proves the bound (23).

The bound (24) follows from (23) applied to ∂_φ . Indeed,

$$\begin{aligned} \|f\|_{(3/2)}^2(\partial\Omega(r)) &= \|f\|_{(1/2)}^2(\partial\Omega(r)) + \|\partial_\varphi f\|_{(1/2)}^2(\partial\Omega(r)) \\ &\leq 3\|f\|_2^2(\Omega(r)) + 3r^2 \|\nabla f\|_2^2(\Omega(r)) + 3\|\partial_\varphi f\|_2^2(\Omega(r)) + 3r^2 \|\nabla \partial_\varphi f\|_2^2(\Omega(r)) \end{aligned}$$

due to (23). Using that $\nabla = (\partial_r, r^{-1} \partial_\varphi)$ and hence

$$|\nabla \partial_\varphi f|^2 = |\partial_\varphi \nabla f|^2 \leq r^2 |\nabla^2 f|^2,$$

we obtain the bound (24).

The proof is complete. \square

Proof of Theorem 3.3. We recall that

$$(25) \quad \|u\|_{(k)}^2(\partial\Omega(r)) = 2\pi r \sum |J_n(t) u_n|^2 (1 + n^2)^k,$$

where u_n are the coefficients of the function $u(r, \varphi)$ in the expansion (16).

First, by using interpolation, a priori constraints, and Lemma 3.4, we will bound $\|u\|_{(1)}(\partial\Omega(r_0))$ by an explicit function of $\varepsilon = \|u\|_2(\partial\Omega(r_0))$.

We observe that according to the constraints (13), (22) and Lemma 3.4 we have

$$\|u\|_{(3/2)}^2(\partial\Omega(r_0)) \leq 3M_0^2 + 6r_0^2 M_1^2 + 3r_0^4 M_2^2 = C_5^2,$$

where the last equality is the definition of C_5 . Using (25) and the Hölder inequality

$$\sum a_n b_n \leq \left(\sum a_n^p \right)^{1/p} \left(\sum b_n^q \right)^{1/q}$$

with $a_n = |J_n u_n|^{2/3}$, $b_n = |J_n u_n|^{1/3}(1 + n^2)$, and $p = 3, q = 3/2$ we will have

$$\|u\|_{(1)}^2(\partial\Omega(r_0)) \leq 2\pi r_0 \left(\sum |J_n u_n|^2\right)^{1/3} \left(\sum |J_n u_n|^2(1 + n^2)^{3/2}\right)^{2/3} \leq \varepsilon^{2/3} C_5^{4/3} = \varepsilon_2^2. \tag{26}$$

Now, by using the differentiated representation (16) and its splitting from the proof of Theorem 3.1 we will bound the normal derivative of u on $\partial\Omega(r_0)$.

We have

$$\partial_r u(r, \varphi) = k \sum J'_n(t) u_n e^{in\varphi}.$$

As in (19),

$$\begin{aligned} \|\partial_r u\|_2^2(\partial\Omega(r_0)) &= 2\pi r_0 k^2 \left(\sum_{|n| \leq n_1} |J'_n/J_n|^2 |J_n u_n|^2 + \sum_{n_1 < |n|} |J'_n|^2 |u_n|^2 \right) \\ &\leq 2\pi r_0 k^2 \left(C_6 \sum_{|n| \leq n_1} n^2 |J_n u_n|^2 + \sum_{n_1 < |n|} \frac{|J_{n-1}|^2 + |J_{n+1}|^2}{2} |u_n|^2 \right), \end{aligned}$$

where $C_6 = \max |J'_n(kr_0)/(nJ_n(kr_0))|^2$ over $|n| \leq n_1$ and where we have used the known identity $J'_n = 1/2(J_{n-1} + J_{n+1})$ [6]. By using (18) we conclude that the second sum is less than

$$\begin{aligned} &\frac{1}{2} \sum_{n_1 < |n|} \left(\frac{t_0}{2}\right)^{2(n-1)} \frac{1}{((n-1)!)^2} \left(1 + \left(\frac{t_0^2}{4n(n+1)}\right)^2\right) |u_n|^2 \\ &\leq \frac{1}{2} \sum_{n_1 < |n|} \frac{4n^2}{t_0^2} (n!)^{-2} \left(\frac{t_0}{2}\right)^{2n} 2|u_n|^2 \leq \frac{16}{t_0^2} \sum_{n_1 < |n|} n^2 |J_n(t_0)|^2 |u_n|^2, \end{aligned}$$

where we used that $t_0^2 \leq 2n + 4$ and $\frac{1}{2n!} \left(\frac{t_0}{2}\right)^n \leq J_n(t_0)$ when $n_1 < n$, due to the choice of n_1 and to (16). Summing up we conclude that

$$\|\partial_r u\|_2^2(\partial\Omega(r_0)) \leq 2\pi r_0 C_0^* \sum n^2 |J_n(t_0)|^2 |u_n|^2 \leq C_0^* \varepsilon_2^2, \tag{27}$$

where $C_0^* = k^2 \max(C_6, \frac{16}{r_0^2})$.

To conclude the proof we use Theorem 3.1 for $\partial_j u$, (26), and (27).

Since $\nabla u = (\partial_r u, r^{-1} \partial_\varphi u)$ we have from (26), (27) that

$$\|\nabla u\|_2^2(\partial\Omega(r_0)) \leq \left(C_0^* + \frac{1}{r_0^2}\right) \varepsilon_2^2. \tag{28}$$

From the constraints (13) and (22) we have

$$\|\partial_j u\|_2(\Omega(r_1)) \leq M_1, \|\nabla \partial_j u\|_2(\Omega(r_1)) \leq M_2.$$

So from the bound (28) it follows by Theorem 3.1 that

$$\frac{r_0}{r} \|\partial_j u\|_2^2(\partial\Omega(r)) \leq C_1(r)(C_0^* + r_0^{-2})\varepsilon_2^2 + C_7(C_0^* + r_0^{-2})^\theta \varepsilon_2^{2\theta},$$

where $C_7 = 4((1 + \frac{2}{r_1})M_1^2 + M_2^2)$. Similarly, applying the second bound of Theorem 3.1 to $\partial_j u$, we obtain

$$\|\partial_j u\|_2^2(\partial\Omega(r_1)) \leq C_1(r_1)(C_0^* + r_0^{-2})\varepsilon_2^2 + C_9\varepsilon_3 - C_8\varepsilon_3\ln(\varepsilon_3),$$

where $C_8 = \max(k^2 M_1^2, M_2^2)\ln\frac{r_1}{r_0}$, $C_9 = C_8(1 - \ln\frac{C_8 r_0}{2C_7})$, and $\varepsilon_3 = -\frac{1}{\ln((C_0^* + r_0^{-2})^{\frac{1}{2}}\varepsilon_2)}$.

The proof is complete. \square

Now we will give numerical values for constants entering the conditional stability bounds of Theorems 3.1 and 3.3. Since these bounds are determined by a-priori constraints (13), (22) we will numerically evaluate the quantities M_0, M_1 for the important and realistic case of the pressure field u generated by the unit point source located at the point q . We consider $q = (1.5, 1.5)$, $r_1 = 1$, and $r_0 = 0.9$ or 0.95 . The choice of geometry, frequencies k , and u simulates the acoustics of an engine near an aircraft cabin Ω . We will consider two solutions u and $u + e$. We will denote by δ the relative error $\frac{\|e\|_2(\partial\Omega(r_0))}{\|u\|_2(\partial\Omega(r_0))}$.

k	$\ u\ _2(\Omega(r_1))$	$\ \nabla u\ _2(\Omega(r_1))$	$\ \nabla^2 u\ _2(\Omega(r_1))$
1	0.0591	0.0661	0.0793
2	0.0301	0.1245	0.5183
3	0.0202	0.1842	1.6865

k	δ	$\frac{\ u-u_\delta\ _2}{\ u\ _2}(\partial\Omega(r))$	$\frac{\ u-u_\delta\ _2}{\ u\ _2}(\partial\Omega(r_1))$
1	0.01	0.4886	0.6034
2	0.01	0.5928	1.2739
3	0.01	0.6834	2.0028
1	0.005	0.3485	0.5706
2	0.005	0.4229	1.2082
3	0.005	0.4872	1.9026

k	δ	$\frac{\ u-u_\delta\ _2}{\ u\ _2}(\partial\Omega(r))$	$\frac{\ u-u_\delta\ _2}{\ u\ _2}(\partial\Omega(r_1))$
1	0.01	0.2762	0.4380
2	0.01	0.3292	0.9295
3	0.01	0.3753	1.4667
1	0.005	0.1829	0.4139
2	0.005	0.2179	0.8808
3	0.005	0.2484	1.3920

In the second table we consider $r_0 = 0.9, r = 0.95$ to compare it with the third table where $r_0 = 0.95, r = 0.97$. While stability is improved when r_0 is closer to 1, these bounds are not very optimistic. They can be improved by using extra regularity assumptions. In our numerical examples reconstruction is much better.

Now by using the previous results in this section we will discuss an optimal choice of the truncation parameter p when recovering pressure u on $\partial\Omega(1)$ from its value $u + e$ on $\partial\Omega(r_0)$. Here e is the error term, $\|e\|_2(\partial\Omega(r_0)) \leq \varepsilon$.

Let $u(;p)$ be the sum (16) truncated over $|n| < p$ and $u_e(;p)$ be a solution of the truncated problem with data $e(;p)$. As in (19), (20), (21), we obtain

$$\|u_e(;p)\|_2^2(\partial\Omega(1)) \leq (C_1(1) + 4r_0^{-2p})\varepsilon^2.$$

According to (25) and (26)

$$\begin{aligned} \|u - u(\cdot; p)\|_2^2(\partial\Omega(1)) &\leq 2\pi \sum_{p < |n|} |u_n J_n|^2 \leq \frac{2\pi}{p} \sum_{p < |n|} n |u_n J_n|^2 \\ &\leq \frac{1}{p} \|u\|_{(1/2)}^2(\partial\Omega(1)) \leq \frac{3}{p} (M_0^2 + M_1^2) \end{aligned}$$

by Lemma 3.4. Hence the error due to solution of the truncated problem does not exceed

$$C_1(1)\varepsilon^2 + 4r_0^{-2p}\varepsilon^2 + 3(M_0^2 + M_1^2)/p$$

and the optimal choice of p corresponds to the minimum of the last sum with respect to p which is achieved at $p = p_{optimal}$. Equating the derivative with respect to p to zero, we will have the equation

$$-8\varepsilon^2 e^{-2p \log r_0} \log r_0 - 3(M_0^2 + M_1^2)/p^2 = 0$$

or $m\varepsilon^m = C_2/\varepsilon$, where $m = -p \log r_0$, $C_2 = (3(M_0^2 + M_1^2)(-\log r_0)/8)^{1/2}$. For example, when $M_0 = 0.5$, $M_1 = 0.5$, $r_0 = 0.9$, and $\delta = 0.005$, we find that $p_{optimal} \approx 20$, which is close to the optimal values of p in the numerical examples below.

4. Numerical solution of the integral equation (4) and regularization methods. In this section, we consider the numerical solution of the integral equation (4) for a range of wave numbers k . Recall that $k = \omega/c$, where ω denotes frequency and c is the speed of sound. In the case of interior aircraft cabin noise $c = 340m/sec$ and the range of interest of ω is typically in the range of human speech,

$$20\pi/sec < \omega = 2\pi f < 1000\pi/sec,$$

where f is frequency in Hertz. This leads to a *range of k* of

$$.06\pi/m < k < 3\pi/m.$$

Since cabin dimensions a are on the order of meters, the dimensionless quantity ka has a similar range.

The numerical algorithms. Here are some details on the numerics. All programming has been done in Matlab and run on Pentium PCs.

Given u on Γ_0 , we solve

$$S\phi = u$$

(or the appropriate least squares problem) for ϕ where we denote by S the integral operator in (4). In order to recover the normal velocities on Γ , we then compute

$$v = D\phi,$$

where D denotes the Fredholm integral operator in (5).

Discretization. For the two-dimensional case, we discretize the integral operators by the N -point Nyström method which is optimal; see, e.g., [2], [5]. For smooth curves the diagonal terms of the integral operator part of D become, essentially,

the curvature. As a result, if the boundary curve Γ is analytic, the discretization of D will exhibit spectral accuracy, with the error roughly squaring each time N is doubled. Similarly, since the kernel of S is analytic, the condition number of the $N \times N$ discretization of S will square each time N is doubled, as expected from the geometric decay of the singular values of S [14, Theorem 15.20]; see the tables below.

Regularization and parameter-choice methods. For data u with noise it is necessary to regularize the solution to filter out high levels of noise in the high frequency modes associated with small singular values of S . According to standard results from, e.g., [6], [7], [12], [14], the theorems developed in the previous sections of this paper guarantee the convergence of the regularized solution as the noise level goes to 0.

We have tested several regularization and parameter selection routines described in [10], [8], [17]. The Matlab package [9] was used in most cases along with the built-in svd routine. We will report on only a few representative calculations here using the truncated svd (tsvd in [9]) and the conjugate gradient method for the normal equations (cgl in [9]). In the case of the truncated svd, the regularization parameter p is the number of singular vectors retained in the reconstruction. More explicitly, we are regularizing the (discretized) least squares problem

$$\min_{\phi} \|S\phi - u^{\delta}\|_2$$

for ϕ , where $u^{\delta} = u + e$, $e = \text{noise}$ with $\|e\|_2/\|u\|_2 = \delta$. The Matlab svd routine computes the singular value decomposition of our $N \times N$ matrix S :

$$S = U\Sigma V^*, \quad U^*U = I, \quad V^*V = I,$$

where $U = [u_1, \dots, u_N]$, $V = [v_1, \dots, v_N]$, $\Sigma = \text{diag}(\sigma_1, \dots, \sigma_N)$, and $\sigma_1 \geq \sigma_2 \geq \dots \geq \sigma_N \geq 0$. The solution to least squares problem is then given by

$$\phi = \sum_{i=1}^{\text{rank}(S)} \frac{u_i^* u}{\sigma_i} v_i + \sum_{i=1}^{\text{rank}(S)} \frac{u_i^* e}{\sigma_i} v_i.$$

The tsvd routine just truncates this solution after the first p terms, filtering out the high frequency noise components which have been amplified by division by small singular values and thus giving the regularized solution:

$$\phi_p = \sum_{i=1}^p \frac{u_i^* u^{\delta}}{\sigma_i} v_i.$$

In the case of conjugate gradient, the regularization parameter p is the number of conjugate gradient iterations. Since conjugate gradient for the normal equations minimizes the S^*S -norm error over the p th Krylov space $K_p(S^*u^{\delta}, S^*S)$ and since

$$\|\phi - \phi_p\|_{S^*S}^2 = \|u^{\delta} - S\phi_p\|_2^2,$$

at each step p conjugate gradient finds the least squares solution ϕ_p over K_p . Note from Figures 2, 3, and 4 that the conjugate gradient method finds the optimal solution in the first several iterations and then diverges rapidly toward the solution to the problem with noisy data. This regularizing behavior is due to the fact that conjugate gradient initially reduces the error in the direction of the dominant (low frequency) singular vectors v_i ($S^*Sv_i = \sigma_i^2 v_i$), which are less corrupted by noise relative to the

high frequency modes corresponding to small σ_i . The rapid convergence/divergence behavior makes the choice of the regularization parameter p (stopping rule or spectral cutoff) crucial.

We have considered various parameter choice methods such as generalized cross validation (gcv in [9]) and the heuristic stopping rule for conjugate gradient given in [8]. If the noise level is known well enough, the discrepancy principle [10] can be used. However, this is generally not the case. A practical possibility in the context of aircraft noise problems is that 20 or so vibrometer measurements of the velocity can be made on Γ . Denoting these measurements v_{meas} , the p can be chosen such that $\|(D\phi_p)_{meas} - v_{meas}\|_2$ (which might be thought of as a penalty term depending on $D\phi$ being added to the least squares problem) is minimized. The results below and in the three-dimensional case indicate that this is a reliable method. The ease with which velocity measurements may be incorporated in the regularization procedure is an advantage of the single layer potential representation.

Numerical examples. We now give results of our numerical calculations for various geometries and various values of k to demonstrate the regularization techniques. Specifically, we use normally distributed random noise with mean 0 and standard deviation 1 from the Matlab random number generator *randn*: $u^\delta = u + e$ where $e = \delta\|u\|_2 f / \|f\|_2$ with $f = \text{randn}(\text{size}(u))$. This gives $\|u^\delta - u\|_2 / \|u\|_2 = \delta$. Our relative errors are given by

$$\|v - v_p\|_2 / \|v\|_2 \leq \text{cond}(D) \|\phi - \phi_p\|_2 / \|\phi\|_2,$$

where ϕ_p is the regularized solution and $v_p = D\phi_p$.

Example 1. Γ (the fuselage) is the unit circle, Γ_0 (the microphone measurement surface) is the circle of radius .9, and the exact u is a point source $u(x, y) = H_0^{(1)}(k|(x, y) - (1.5, 0)|)$. The exact velocity v on Γ can be computed easily from u . The following table indicates how the relative errors in v_p for the optimal p (in parentheses in the tables), which we know from the exact v , change for various noise levels δ . We see that as $\delta \rightarrow 0$ the relative error approaches 0, as expected from the theory. The condition numbers, $\text{cond}(S)$ and $\text{cond}(D)$, for each N are given in the 2-norm. D is well conditioned, as expected, unless k is very near to an eigenvalue which does not usually cause a problem in practice. $\text{cond}(D) \approx 1.2$ for all N and $\sigma_1(S)$ is of order 1, so σ_N is of order $1/\text{cond}(S)$. Note that for $\delta = 0$ the error roughly squares each time N is doubled, as expected by the spectrally accurate Nyström discretization of S , until the amplification of the rounding error ($\approx 10^{-16}$ in Matlab) by the small singular values of S overwhelms the truncation error for $N = 320$.

N	$\text{cond}(S)$	$\delta = .05(p)$.01	.001	.0001	0
20	$2.7 \cdot 10^1$.15(11)	.089(12)	.048(20)	.047(20)	.036(20)
40	$1.6 \cdot 10^2$.18(9)	.060(19)	.017(23)	.0037(33)	.0027(40)
80	$2.6 \cdot 10^3$.13(13)	.055(16)	.011(24)	.0026(31)	$1.7 \cdot 10^{-5}$ (80)
160	$3.6 \cdot 10^5$.11(10)	.037(20)	.0095(26)	.0019(33)	$2.9 \cdot 10^{-9}$ (160)
320	$3.0 \cdot 10^9$.12(10)	.038(18)	.0095(25)	.0019(33)	$3.6 \cdot 10^{-8}$ (100)

Example 2. Γ (the fuselage, solid curve in Figure 1) is the ellipse $(x, y) = (\cos(\theta), .5 \cdot \sin(\theta))$, Γ_0 (the microphone measurement surface, dotted curve in Figure 1) is the ellipse $(x, y) = .9 \cdot (\cos(\theta), .5 \cdot \sin(\theta))$, and the exact u is the sum of 2 sources (representing “engines” on either side of the fuselage) $u(x, y) = H_0^{(1)}(k|(x, y) - (.5, 1)|) + H_0^{(1)}(k|(x, y) - (.5, -1)|)$. The “O” symbols on the fuselage indicate the po-

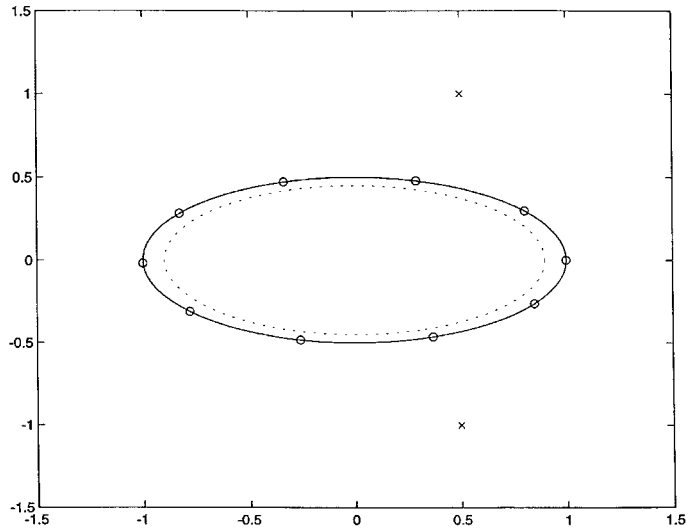


FIG. 1.

sitions of 10 velocity measurements, v_{meas} . Our results for $\delta = .01$, a realistic noise level in practice, are exhibited in the following table and in Figures 2, 3, and 4 which plot the relative errors in v (with $N = 80$) for the tsvd (solid line) and the conjugate gradient iterations (dashed line) against p , along with the relative errors in v_{meas} for the tsvd (dotted line) and the conjugate gradient iterations (dot-dash line). The “O” symbol indicates the point picked by gcv. Note, e.g., for Figure 2, that the gcv point is quite sensitive to rapid changes in the relative error and can be far from the optimal solution in such cases. As k increases, S becomes better conditioned and there is more margin for error in the search for the optimal p . The plots show that choosing p such that the error in v_{meas} is minimized should give a reliable parameter choice method in either case. For large scale three-dimensional problems especially, the conjugate gradient method is much faster than the tsvd, since it finds the optimal solution in the first several iterations. Figure 5 compares the absolute value of the exact and regularized velocities for tsvd and conjugate gradient for $k = 6$.

The following table gives some indication how the relative errors vary with N and k . $\text{cond}(D)=2.9$ for $k = 1$, 5.6 for $k = 3$, and 16 for $k = 6$. (Note that for $N = 320$, the condition number is not accurately computed.) We observe that, in general, for 1% noise, we cannot expect much more than about 3% accuracy in the regularized solution in the 2-norm. Pointwise errors may be somewhat better.

N	$\text{cond}(S)$	$k = 1$	$\text{cond}(S)$	$k = 3$	$\text{cond}(S)$	$k = 6$
20	$1.1 \cdot 10^2$.13(8)	$4.2 \cdot 10^1$.088(16)	$2.1 \cdot 10^1$.18(20)
40	$2.2 \cdot 10^3$.082(11)	$8.8 \cdot 10^2$.040(19)	$4.8 \cdot 10^2$.050(28)
80	$3.0 \cdot 10^7$.071(10)	$1.2 \cdot 10^7$.032(19)	$6.7 \cdot 10^6$.041(27)
160	$1.8 \cdot 10^{18}$.046(17)	$1.1 \cdot 10^{18}$.029(19)	$2.3 \cdot 10^{17}$.029(29)
320	$3.5 \cdot 10^{18}$.052(17)	$1.7 \cdot 10^{18}$.024(23)	$4.8 \cdot 10^{17}$.029(35)

Example 3. Figure 6 compares the absolute value of the exact (V) and recovered velocities (VREC) for a region bounded by a circle intersected by a straight line. This is meant to simulate the cross section of a fuselage with a floor, as in [22], and is

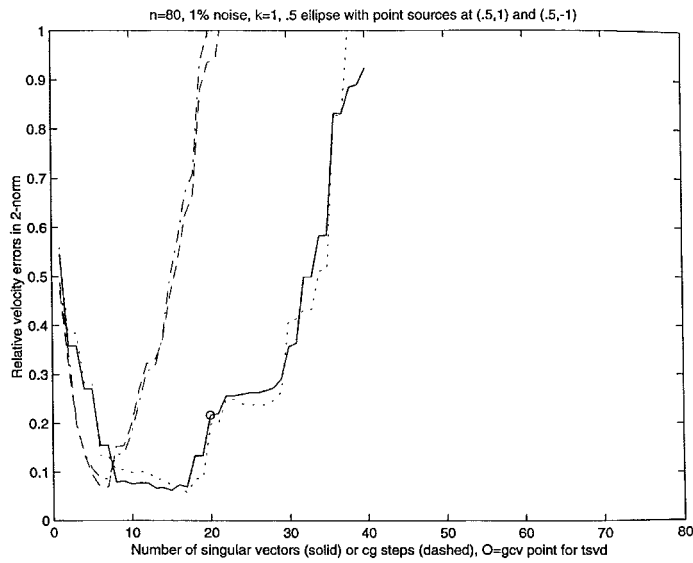


FIG. 2.

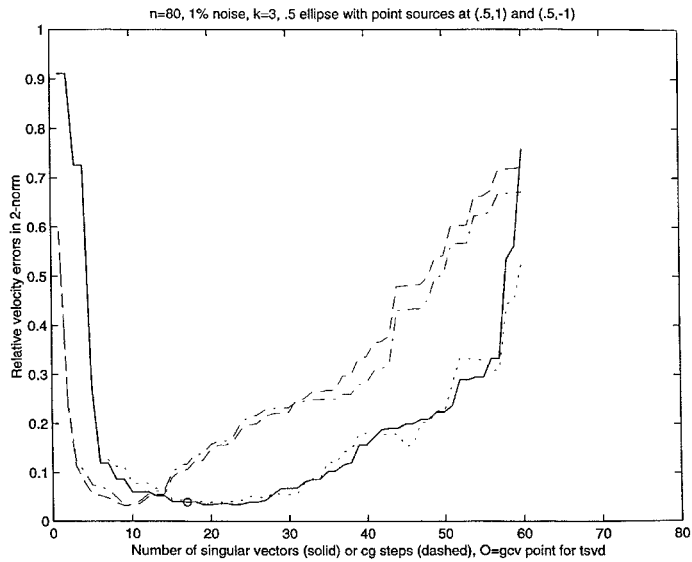


FIG. 3.

representative of the kind of nonsmooth boundaries that may arise in practice. Even in this case, the recovered, regularized velocities approximated the exact velocities well away from the corners.

Concluding remarks. We have also developed a three-dimensional code based in part on triangulation of the boundary surface and piecewise-polynomial boundary elements in [1] and [2]. We have carried out a number of numerical experiments with results similar to the two-dimensional case. Computations similar to ours using the Helmholtz–Kirchhoff representation, series expansions, or a hybrid layer potential are

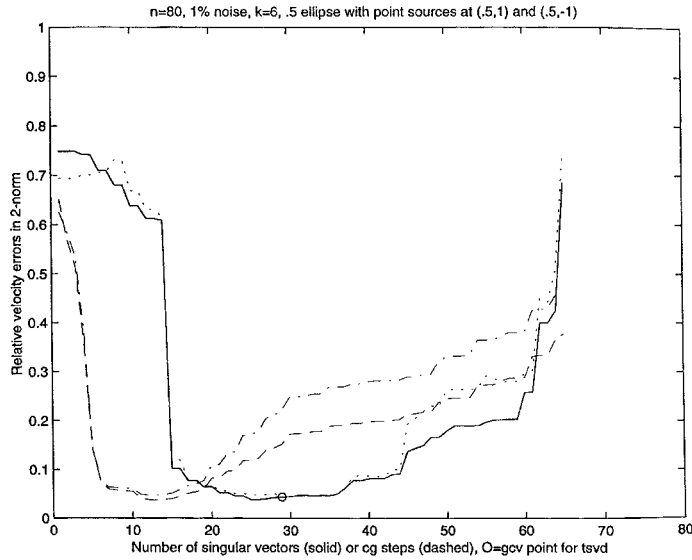


FIG. 4.

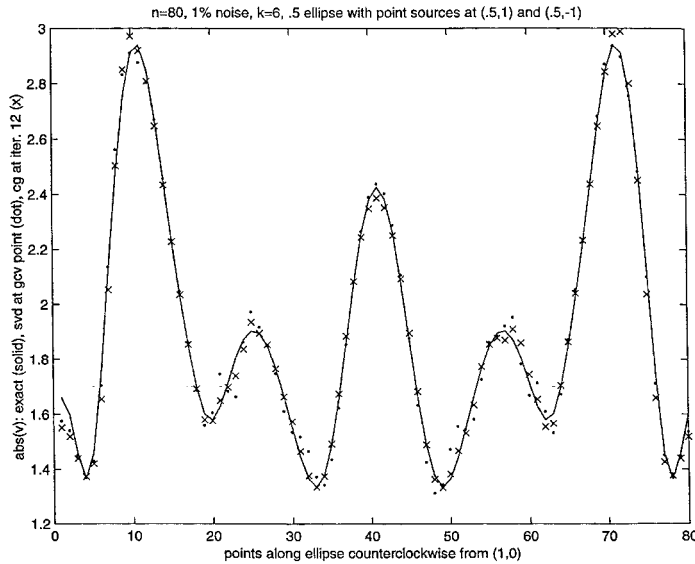


FIG. 5.

given in [3], [13], [16], [22], [23]. We plan to compare these methods and those of [18] with ours and to report more fully on our computations using test problems and experimental data taken from a fuselage test section in future work.

The results of these experiments show that the single layer representation can be used for efficient numerical algorithms. The reconstruction error is reasonably low and is decreasing as the frequency grows from 1 to 3, which is acoustically the most interesting interval where most of the acoustical energy is concentrated. In later work we plan to show that stability is increasing with frequency. On the other hand, higher

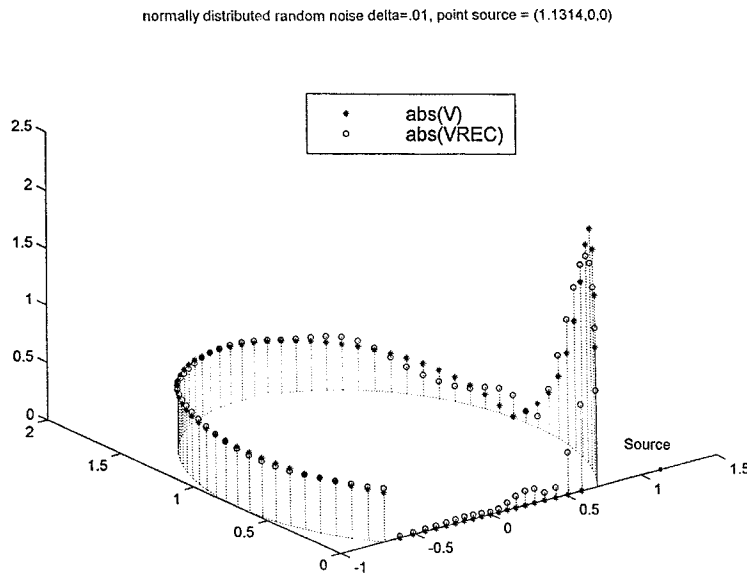


FIG. 6.

frequency generates serious computational problems and we plan to resolve them by using preconditioners and more accurate discretization of integrals.

REFERENCES

- [1] K. E. ATKINSON, *User's Guide to a Boundary Element Package for Solving Integral Equations on Piecewise Smooth Surfaces, Release 2*, University of Iowa, Iowa City, IA, 1998.
- [2] K. E. ATKINSON, *The Numerical Solution of Integral Equations of the Second Kind*, Cambridge University Press, Cambridge, UK, 1997.
- [3] M. R. BAI, *Application of BEM (boundary element method)-based acoustic holography to radiation analysis of sound sources with arbitrarily shaped geometries*, J. Acoust. Soc. Amer., 92 (1992), pp. 533–549.
- [4] G. V. BORGOTTI, A. SARKISSIAN, E. G. WILLIAMS, AND L. SCHUETZ, *Conformal generalized near-field acoustic holography for axisymmetric geometries*, J. Acoust. Soc. Amer., 88 (1990), pp. 199–209.
- [5] D. COLTON AND R. KRESS, *Integral Equation Methods in Scattering Theory*, Wiley, New York, 1983.
- [6] D. COLTON AND R. KRESS, *Inverse Acoustic and Electromagnetic Scattering Theory*, Springer-Verlag, New York, 1992.
- [7] H. W. ENGL, M. HANKE, AND A. NEUBAUER, *Regularization of Inverse Problems*, Kluwer, Dordrecht, the Netherlands, 1996.
- [8] M. HANKE, *Conjugate Gradient Type Methods for Ill-Posed Problems*, Pitman Res. Notes Math. Ser. 327, Longman Scientific and Technical, Harlow, UK, 1995.
- [9] P. C. HANSEN, *Regularization Tools: A Matlab Package for Analysis and Solution of Discrete Ill-Posed Problems*, version 2.0 for Matlab 4.0 (1992, revised 1995); see Numer. Algorithm, 6 (1994), pp. 1–35; software available via netlib@research.att.com from directory NUMER-ALGO.
- [10] P. C. HANSEN, *Rank-Deficient and Discrete Ill-Posed Problems: Numerical Aspects of Linear Inversion*, SIAM, Philadelphia, 1997.
- [11] V. ISAKOV, *Inverse Source Problems*, Mathematical Surveys and Monographs 34, AMS, Providence, RI, 1990.
- [12] V. ISAKOV, *Inverse Problems for Partial Differential Equations*, Springer-Verlag, New York, 1998.

- [13] B.-K. KIM AND J.-G. IH, *On the reconstruction of the vibro-acoustic field over the surface enclosing an interior space using the boundary element method*, J. Acoust. Soc. Amer., 100 (1996), pp. 3003–3016.
- [14] R. KRESS, *Linear Integral Equations*, Springer-Verlag, New York, 1992.
- [15] C. MIRANDA, *Partial Differential Equations of Elliptic Type*, Springer-Verlag, New York, Berlin, 1970.
- [16] A. TEKATLIAN, P. FILIPPI, AND D. HABAUT, *Determination des caracteristiques vibratoires de sources de bruit par resolution d'un probleme inverse de rayonnement*, ACUSTICA, 82 (1996), pp. 91–101.
- [17] C. R. VOGEL AND J. G. WADE, *Iterative SVD-based methods for ill-posed problems*, SIAM J. Sci. Comput., 15 (1994), pp. 736–754.
- [18] E. G. WILLIAMS, *Fourier Acoustics: Sound Radiation and Nearfield Acoustical Holography*, Academic Press, New York, 1999.
- [19] E. G. WILLIAMS, *On Green's function for a cylindrical cavity*, J. Acoust. Soc. Amer., 102 (1997), pp. 3300–3307.
- [20] E. G. WILLIAMS, *The nearfield acoustical holography experimental method applied to vibration and radiation in light and heavy fluids*, Comput. & Structures, 65 (1997), pp. 323–335.
- [21] E. G. WILLIAMS AND B. H. HOUSTON, *New Green Functions for Nearfield Acoustical Holography in Aircraft Fuselages*, AIAA paper 96-1703, State College, PA, 1996.
- [22] E. G. WILLIAMS, B. H. HOUSTON, P. C. HERDIC, R. RAVEENDRA, AND B. GARDNER, *Interior NAH in flight*, J. Acoust. Soc. Amer., 108 (2000), pp. 1451–1463.
- [23] S. F. WU AND J. YU, *Reconstructing interior acoustic pressure fields via Helmholtz equation least-squares method*, J. Acoust. Soc. Amer., 104 (1998), pp. 2054–2060.